Neurocomputing 461 (2021) 679–695

Contents lists available at ScienceDirect

Neurocomputing

journal homepage: www.elsevier.com/locate/neucom

Routes to tripod gait movement in hexapods

R. Barrio [a,*], Á. Lozano [b], M.A. Martínez [a], M. Rodríguez [c], S. Serrano [a]

[a] IUMA, CoDy and Dpto. Matemática Aplicada, Universidad de Zaragoza, E-50009 Zaragoza, Spain
[b] IUMA, CoDy and Centro Universitario de la Defensa, Academia General Militar, Universidad de Zaragoza, E-50090 Zaragoza, Spain
[c] CoDy and Dpto. Matemática Aplicada, Universidad de Zaragoza, E-50009 Zaragoza, Spain

ARTICLE INFO

Article history:
Received 18 December 2019
Revised 19 May 2020
Accepted 21 June 2020
Available online 13 May 2021

Keywords:
Insect movement gaits
CPGs
Neuronal networks
Bifurcations
Tripod gait

ABSTRACT

The use of hierarchical networks in motor pattern generation in hexapod robots and in insect movement provides ways to understand and control both systems. In this paper we consider the Central Pattern Generator (CPG) of insect movement consisting of six coupled neurons developed by Ghigliazza and Holmes (2004) that produces the global leg coordination pattern. We provide a detailed study of the possible gaits generated by the CPG through different numerical techniques recently developed for the study of small networks, which allow us to consider the complete model without any simplification. We combine the analysis of isolated neurons (using several three dimensional parameter spaces) to give a roadmap of the dynamics of the neurons involved, lateral phase lag plots to show the convergence and transitions towards particular patterns and a quasi-Monte Carlo sweeping method to describe different pattern routes in the parametric phase space. In all of our studies we have found the same final result: most of the observed patterns follow routes that lead to the stable tripod gait. We obtain several routes made of symmetrical patterns, but despite considering mainly a symmetric leg CPG we detect non-symmetrical patterns that provide (minor) routes present in the model. The bifurcations of the main pattern routes detected in the parameter space are studied in detail using continuation techniques. This study reveals the bifurcations that create and destroy the different routes and how for large values of some parameters only the tripod gait is present. Based on the symmetric case, a preliminary study of asymmetric configurations is done revealing the robustness of the already located patterns and routes. Due to the relevance of the tripod gait, and since more parameters are included in this study, we introduce an algorithm to locate the limit of the tripod gait in the parameter space, which shows that there is a large three parametric region where the tripod pattern is ubiquitous and highly dominant in rapidly moving insect regimes.

1. Introduction

The study of patterns in networks is nowadays a current research line due to the large number of practical applications. Most of the articles consider, as the basic model, networks of oscillators [1–4], but recently the use of more particular models is growing, like in the study of Central Pattern Generators (CPGs), which are neuronal circuits that when activated can generate rhythmic motor patterns even in absence of sensory input [5–8]. Their dynamics depends on intracellular, synaptic, and network level phenomena. The study of networks of oscillators is done combining different techniques, and besides, its simple formulation allows also some powerful analytical tools like the Ott-Antonsen ansatz [9] to reduce large networks to a low dimensional mean field.

In the case of generic small networks we have recently proposed [10] two numerical techniques to deal with small neuron CPGs. In this paper we use these techniques to detail the location of the different gait patterns in insect movement taking into account different parameters (instead of just one as in [10]). In fact, the goal is to describe how the system network can change in order the insect reaches the tripod gait. During tripod gait, three legs move at a time while the other three remain stationary, that is, three legs are always on the ground. In the design of robots, a typical approach consists of using wheeled or tracked locomotion, but those with legs are able to operate on irregular terrain. They can alter various stages and aspects of their gaits in order to compensate irregularities on the ground. For that reason, there is a growing interest in using insect locomotion schemes to control walking

* Corresponding author.
E-mail addresses: rbarrio@unizar.es (R. Barrio), alozano@unizar.es (Á. Lozano), gelimc@unizar.es (M.A. Martínez), marcos@imark.es (M. Rodríguez), sserrano@unizar.es (S. Serrano).

https://doi.org/10.1016/j.neucom.2020.06.151
0925-2312/

robots. Several models for insect locomotion exist based mainly on a six-neuron CPG (see [11–14]), and robotics researchers [15–20] also use similar simplified models. Insects in nature often run using tripod pattern. At a moderate speed, insects use different gaits like ripple gait, wave gait and tetrapod gait. These gaits allow the animal to slow down to observe the surroundings, but fast motion is usually based on tripod gaits due to its speed and stability. The main questions are: how the different gaits evolve towards the stable tripod gait? Is it possible to locate the region of dominant tripod gait in the space of parameters? These questions may also help to hexapodal robots movement [15,17,20] in order to design suitable gait changes.

In this paper we consider a CPG with six coupled neurons following the model developed by Ghigliazza and Holmes [14]. In that work, the neural architecture of cockroach locomotion was described by the bursting model developed in [22] along with a single equation describing synaptic dynamics. See Section 2 and the Appendix for a short description of the CPG model. Since the neuron model is four dimensional, the complete CPG model is an ODE system of dimension 24. In order to perform an analysis of such systems, several simplification approaches are commonly used. The only limitation of these approaches is that they introduce simplifications that do not cover numerous non-symmetric patterns. For example Fig. 1 shows some non-symmetric patterns illustrating a hypothetical relation between the various six-legged gaits (figure, caption and explanation adapted from Fig. 1 in Wilson, 1966 [21]). The solid bars indicate protraction (leg off ground and moving forward relative to the body and ground). For the purpose of making the simplest presentation, protraction time and interstep intervals between legs 3 to 2 and 2 to 1 are held constant and frequency changes are accomplished by varying only the interval between stepping in leg 1 and leg 3. Legs on opposite sides in the same segment are held in strict antiphase. Dotted enclosures indicate fixed basic sequences of steps of the legs of one side. In (a), the lowest frequency pattern is shown. Each leg steps by itself. In (b), the basic sequences overlap and some legs step in pairs (dashed enclosures). In (c) and (d), the sequences overlap more. In order to have the sides alternate strictly, legs cannot step in exact pairs. Dashed enclosures indicate nearest temporal neighbor pairs. In (e), further overlap results in the tripod gait. Even the sequences on one side overlap so that legs 1 and 3 synchronize. In (f), at the highest frequency, the sequence beginning with leg 3 starts before the end of the previous sequence, so there is an apparent reversal of the direction of the stepping sequence (dashed enclosures). Some of these patterns have been experimentally found in insects. The study of their appearance or not on mathematical models may provide mechanisms to control and explain them. In a previous work [10], the insect movement CPG was used as example for two different techniques introduced to study small networks, *lateral phase-lag analysis* and a *quasi-Monte Carlo sweeping*. In this work we use these techniques to expand the analysis to other parameters and we focus on how the dominant patterns evolve towards tripod movement obtaining a surface tripod limit in a three dimensional parameter space. Moreover, in literature there is no global study of the mechanisms that explains why the observed pattern appear or disappear, that is, the involved bifurcations. To answer this important question, in this article we study in detail the bifurcations of the main pattern routes detected in the parameter space using continuation techniques via the AUTO software [23,24]. Our study reveals the bifurcations that create and destroy the different routes and what is highly relevant, it shows how for large values of some parameters only the tripod gait is present [25]. Based on the symmetric case a preliminary study of asymmetric configurations is done revealing the robustness of the

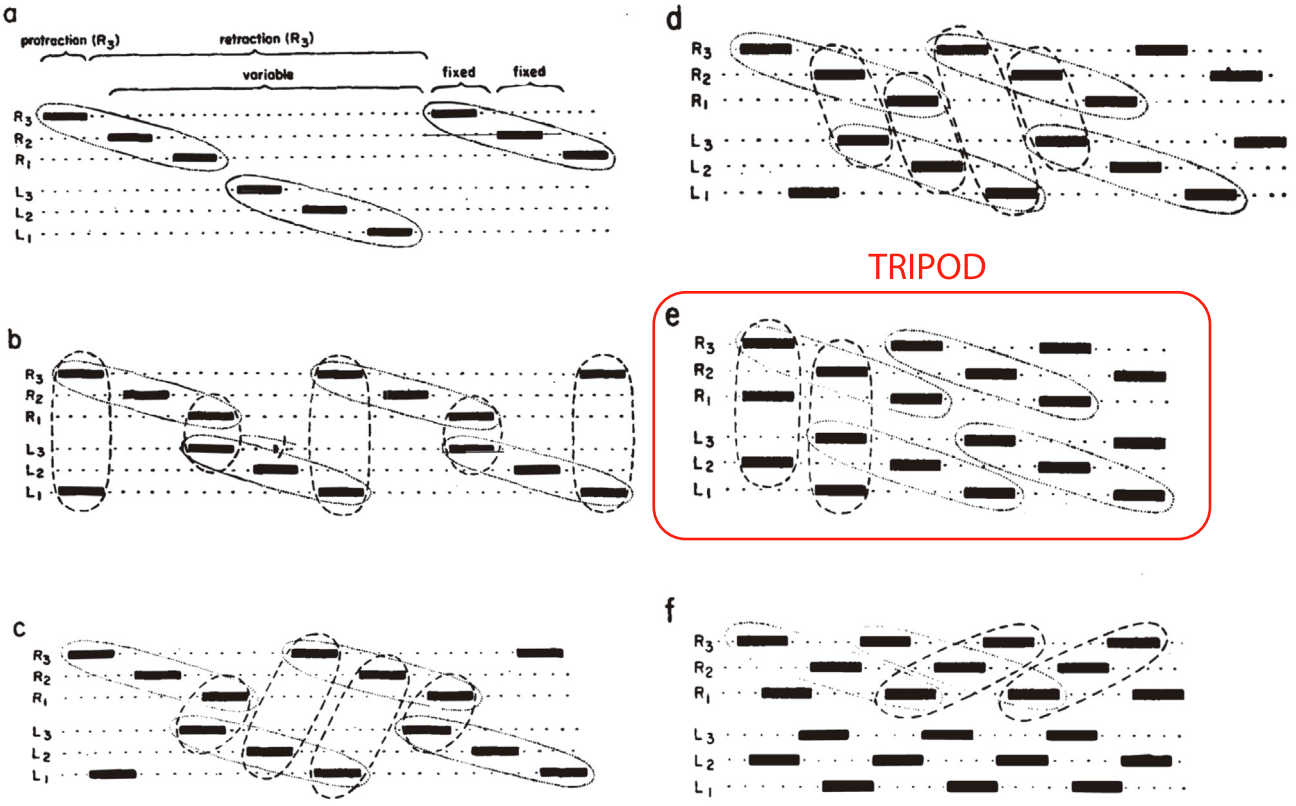

Fig. 1. (Adapted from caption and pictures of Fig. 1 in Wilson, 1966 [21]) Diagram illustrating a hypothetical relation between the various six-legged gaits. The horizontal axis represents time. See explanation in the text.

routes already located. Along this paper we will abuse the notation by calling the same name a specific gait pattern and its route, that is, the parametric evolution of it.

This paper is organized as follows. In Section 2 the neuron and the complete CPG model of insect movement are explained. In Section 3 we focus on the tripod gait movement, firstly showing the different routes to tripod for a particular case, next studying in detail the bifurcations on the different routes. Besides, we study the perturbed case when some asymmetric CPGs are considered, and later we propose an algorithm for the location of the tripod gait limit in parameter space. Finally, in Section 4 some conclusions are presented.

2. Preliminaries

In this paper, we study a CPG that models the insect movement (following the formalism of [14,26]): a network of six mutually inhibiting identical neurons each driving a leg of a cockroach. Fig. 2 shows a representation of the complete CPG and the relation with the different legs of the insect. This model assumes that inhibitory coupling is achieved via synapses that produce negative postsynaptic currents (we obtain this by subtraction of positive postsynaptic currents instead of adding negative terms as in the original model). Other currents included in the model are a fast nonlinear calcium current, I_{Ca}, a slower potassium current I_K, an additional very slow current I_{KS}, a linear leakage current I_L and an external current I_{ext}. Following [14] we include only nearest neighbor coupling and (for the main analysis) lateral symmetry, so that there are three contralateral coupling strengths (c_1, c_2, c_3 in Fig. 2) and four ipsilateral coupling strengths (c_4, c_5, c_6, c_7 in Fig. 2). All connections are inhibitory, i.e. all c_i are positive. The complete model of the CPG is described by an ODE system of dimension 24:

$$\left\{\begin{array}{ll} C\dot{v}_i & = -[I_{Ca}(v_i) + I_K(v_i, m_i) + I_L(v_i) \\ & \quad + I_{KS}(v_i, w_i)] + I_{ext} - (I_{syn})_i(v_i, s_j), \\ \dot{m}_i & = \frac{\epsilon}{\tau_m(v_i)}[m_\infty(v_i) - m_i], \\ \dot{w}_i & = \frac{\delta}{\tau_w(v_i)}[w_\infty(v) - w_i], \\ \dot{s}_i & = \alpha s_\infty(v_i)(1 - s_i) - \beta s_i, \end{array}\right. \tag{1}$$

with $i = 1, 2, \ldots, 6$. Here, v_i are voltages, m_i and w_i are gating variables and s_i are the synapses variables. Parameters C, ϵ and δ, determine the time scales of v, m and w. Parameters α and β are voltage-independent forward and backward rate constants. Detailed expressions for the different auxiliary elements that configure the equations are given in the Appendix.

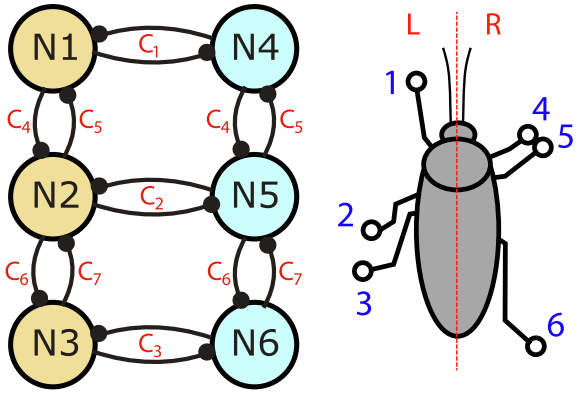

Fig. 2. Complete symmetric CPG model and the relationship between each neuron and the legs of the insect.

Before studying the different movement gait patterns that occur in the CPG model, we study the isolated neuron model (basic unit that makes up the CPG) because it will allow us to develop a roadmap that guides the changes in the different gaits and to know where to analyze the full model of the CPG. So, we take just $i = 1$, the three first variables and $I_{syn} = 0$, to get the 3D model of one isolated motoneuron.

In order to know how the roadmap changes when some model parameters are modified, Fig. 3 shows the results obtained with the spike-counting technique [27,28], leaving different parameters free. We use as bifurcation parameters I_{ext}, v_{KS}^{th}, v_{Ca}^{th}, v_K^{th} and $k_{0_{Ca}}$. The spike-counting technique (it assign a different color to each number of spikes in the stable bursting periodic orbit) shows that the studied plates obtained by changing the first four parameters have qualitatively analogous results, forming a 4-dimensional object in the space of parameters with a band structure inside, each one corresponding to a burster with a fix number of spikes. In addition, these images show us the directions (increasing or decreasing the parameter values) along which the number of spikes increases, and therefore also the duty cycle (ratio between the active interval and period of the orbit) of the burster. Notice that, as the value of the parameter $k_{0_{Ca}}$ increases, the bursting region decreases in size and the number of spikes is also reduced. Moreover, a region with chaotic behavior is clearly present and increases its size as $k_{0_{Ca}}$ grows.

We observe in Fig. 3 that the main characteristics of the model, that is, the bursting frequency, spiking frequency and the duty cycle can be easily modulated by changing most of the parameters, and so we can use I_{ext}, v_{KS}^{th} or v_K^{th} as our main parameters. Note, as indicated in [14], that the bursting frequency and duty cycles of CPG interneurons are the main responsible for speed adjustment, while spiking frequencies are involved in force production. Therefore, we will focus on the changes of bursting frequency and duty cycles since our aim is to study the different gait patterns. So, we set the values $v_{Ca}^{th} = -1.2$ and $k_{0_{Ca}} = 0.055$ where the bursting dynamics are clearly observed (see Eq. (2) in the Appendix). The circled values on the axis of the figures are the chosen ones.

3. Routes to tripod

Consider a neuron network with fixed parameters. To compute the set of possible stable states of that system one could sweep the (meaningful) initial condition space. Since this set is a cube in $\mathbb{R}^{24}$, it is computationally infeasible to perform a systematic sweep along all dimensions. In [10] two different and complementary strategies were developed: on the one hand, select a two-dimensional subspace to take the initial conditions and study the evolution of the phase lag between the neurons (*lateral phase lag analysis*); on the other hand, sweep the initial conditions cube using Monte Carlo method with Halton sequences sampling [29] (*quasi-Monte Carlo sweeping method*).

The *quasi-Monte Carlo sweeping* method (see [10] for a complete description) consists of generating n different sets of initial conditions for each set of fixed parameter values. They are selected in a Halton sequence sampling (deterministic but with low discrepancy) covering the range of each variable, that is $[-40, 10]$ for v_i and $[0, 1]$ for the remaining gating variables. This process is repeated for each neuron of the network. After a big enough transient time, we start computing the pattern produced by the network and the state of the network in a given instant is stored. Later, each sequence is analyzed using the Fast Fourier Transform to detect periodicity, storing them into a list. Finally those patterns which represent the same signal (or its symmetrical) should be detected to output only a representative of its class of equivalence. Now we can estimate the *size* of the attraction basin of each stable pattern as the fraction of initial conditions converging to it. This

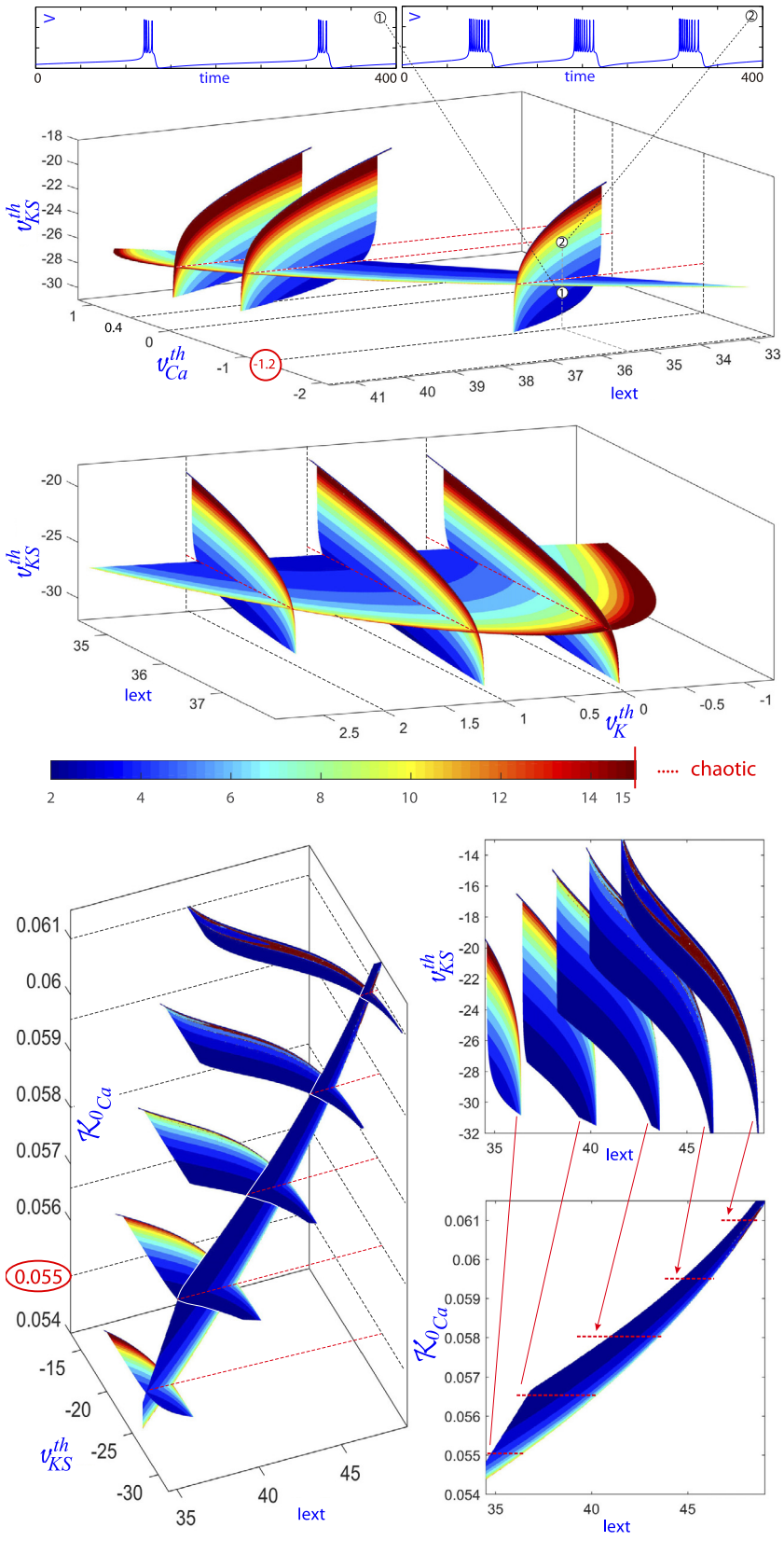

Fig. 3. Three different three parametric analysis (five parameters involved) for the isolated neuron model showing the bursting regions. Different colors (see central bar) represent different number of spikes in the orbit (spike-counting technique) to which the dynamics of the system is attracted for each point of the parametric space when starting from fixed initial conditions. All computed sections show a similar behavior except when the value of the parameter $k_{0_{Ca}}$ increases (bottom picture). In that case, the number of spikes in the periodic orbits decreases and the region with chaotic behavior (dark red color) increases in size while the bursting region decreases.

process has been done for a single set of parameters. If we slightly change one of them we can map the computed classes for one parameter value to the ones of the other values, showing in that way how patterns evolve, for more details, see [10].

Lateral phase lag analysis is based on representation of the delay in the movement between two different legs. Specifically, the delay between the first and third leg with respect to the second (ϕ_{12} and ϕ_{32}, respectively) and the delay between the fourth and sixth leg with respect to the fifth (ϕ_{45} and ϕ_{65}, respectively). Actually, in the phase diagram we represent the normalized phase lag ($d_{ij} = \phi_{ij}/P$) where P is the period of the bursting cycle. We consider always as reference for the delay the middle neurons, that is, numbers N2 and N5, but we should consider also a delay between the two middle neurons. Its temporal evolution is represented in a third (central) diagram. See [10] for a more detailed explanation.

3.1. Routes to dominant tripod gait movement

Before analyzing the routes that lead us to the tripod gait, we will first show the two ends of those routes. In this way we can see how the situation in both cases is very different.

The top panels of Fig. 4 show two phase delay diagrams corresponding to $v_{KS}^{th} = -28$ (left) and $v_{KS}^{th} = -25$ (right), both with $I_{ext} = 35.5$ and $v_K^{th} = 2$, and two central pictures with the temporal evolution of the phase lag between both central neurons. In the upper left panel we can see three stable patterns and two unstable (one saddle and one repulsor), as well as the evolution of the CPG starting from different initial conditions and converging to stable patterns. For example, if we are in the point representing route R1 in the picture, the normalized delay from first to second leg is $d_{12} = 0.2$ meanwhile $d_{32} = 0.8$ and symmetrically, $d_{45} = 0.2$ meanwhile $d_{65} = 0.8$, but we should not forget the delay between the two middle neuron ($d_{52} = 0.2$) (in the small plot inserted). The time series and block representation of voltages of CPG for this pattern are represented in the bottom panels. The point of the route R1′ represents the symmetric pattern with $d_{12} = d_{45} = 0.8$ and $d_{32} = d_{65} = 0.2$. The repulsor pattern corresponds with the tripod gait. We can see the representation of other patterns on Fig. 5.

If we move forward in v_{KS}^{th}, we observe that the activation period is longer because it contains more spikes (as explained in top panel of Fig. 3) but the period becomes shorter. The right panels show a situation where the pattern corresponding with the tripod gait

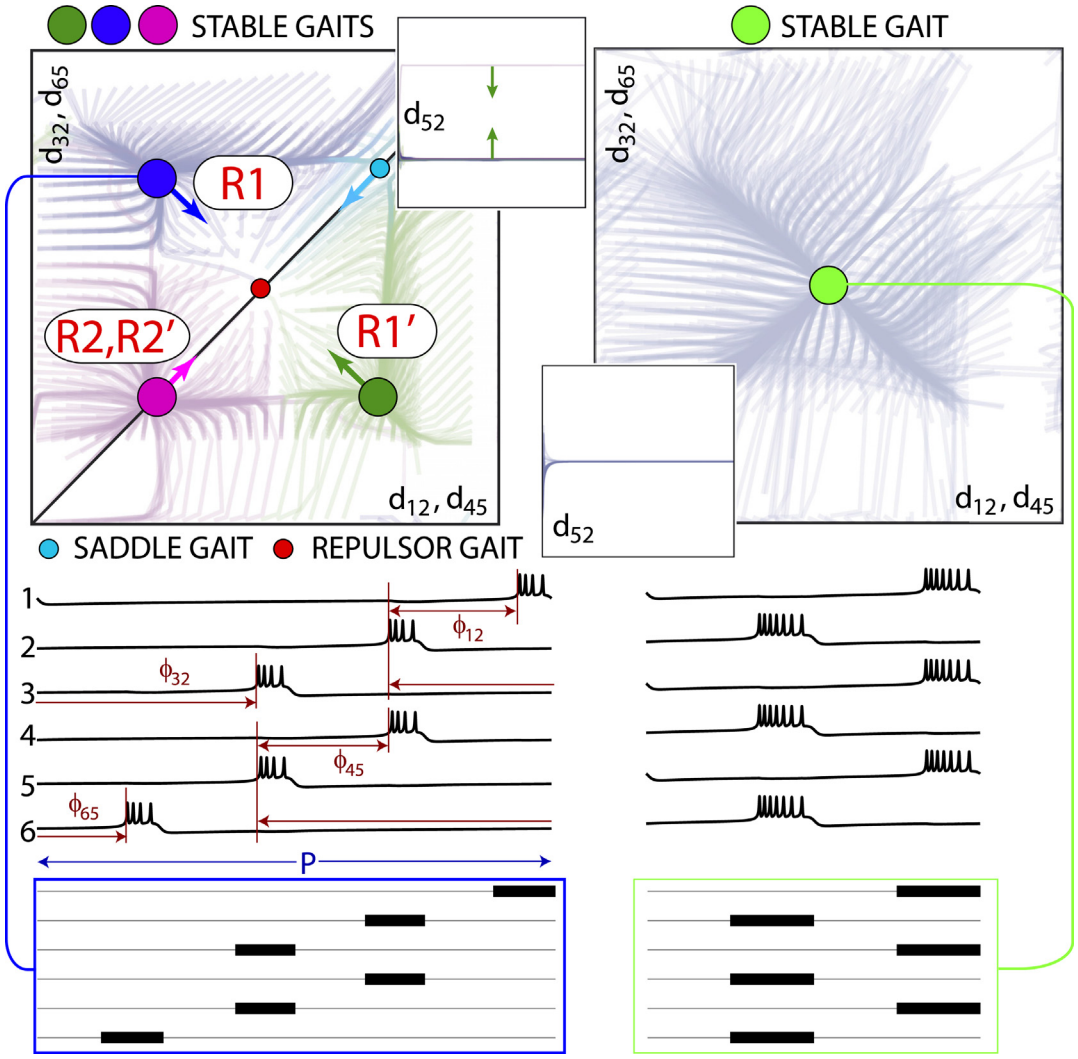

Fig. 4. On the top panels the phase delay diagrams corresponding to $v_{KS}^{th} = -28$ (left) and $v_{KS}^{th} = -25$ (right) both with $I_{ext} = 35.5$ and $v_K^{th} = 2$ and two central pictures with the temporal evolution of the phase lag between both central neurons. In the middle panels the temporal series of the CPG. ϕ_{ij} corresponds to the absolute phase lags between the i and the j neuron while d_{ij} is the normalized one with respect to the period (P) of the bursting cycle. In the bottom panels we show the hexagrams corresponding to the same gait patterns, both as time series or block representation (black rectangles mark time and duration of activation period for each neuron).

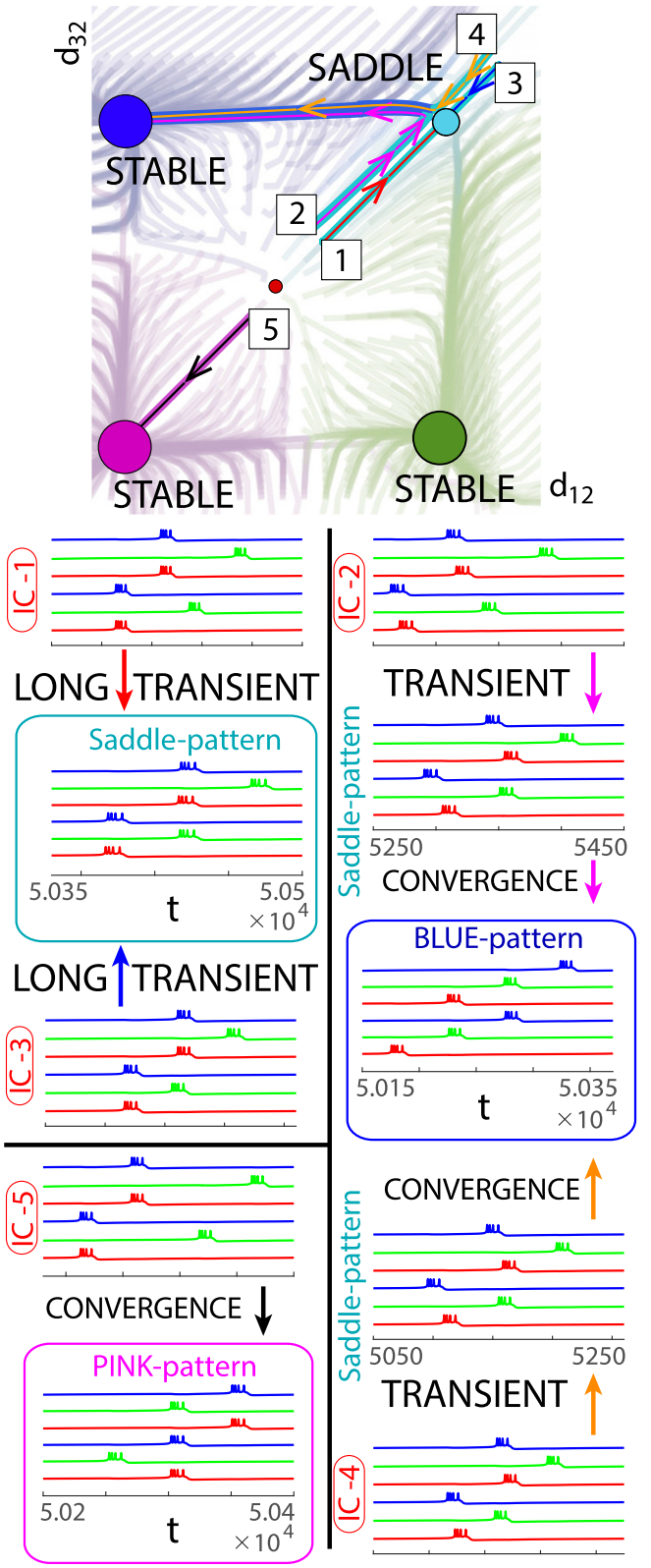

Fig. 5. Time evolution of some initial data of the central part of the phase delay diagram of left panel of Fig. 4. Orbits 1–4 stay some transient time on the saddle-pattern. Orbit 5 converges towards the stable pink pattern dot. See more details in the text.

(repulsor in the left panels) has become stable and it is the only fixed pattern that appears in the phase delay diagram.

As we have stated before, the representation obtained with this method allows us to see the evolution of the CPG from the different initial conditions considered. Therefore, it allows us to obtain the intersection of the basins of attraction of the stable patterns with the subspace selected for the initial conditions. So the dots in the dark blue zone correspond to initial conditions that will evolve towards the stable pattern R1. In the same way with the green and pink zones for patterns R1′ and R2, respectively.

Transient regimes are also key regimes for CPG function, in particular for locomotion, as animal survival depends on them, e.g., for hiding and hunting behaviors. Analyses of the duration of these transients and the ability for transitions between different gaits are crucial, also for robotics. By analyzing the different regions of attraction and the behavior of lines passing near their limits, we can determine the nature of unstable patterns within the selected subspace. Thus, for example, we can determine that the segment $d_{12} = d_{32}$, with $1/2 < d_{12} < 1$, belongs to the stable manifold of the light blue saddle pattern. Therefore, initial conditions very close to this segment will pass very close to the light blue saddle pattern and may be close to it for an indefinitely long time. This circumstance is shown in Fig. 5, where the initial conditions 1 and 3, located on that segment, quickly evolve towards the saddle pattern and hold there during a very long transient (more than $5 \cdot 10^4$ milliseconds). Initial conditions 2 and 4, being a little further from the stable manifold, pass close to the saddle pattern for a short transient time and then converge to pattern R1 (dark blue). As an example of a different situation, we show the evolution of the CPG from the initial conditions 5. In this case, given the location of the initial conditions clearly within the basin of attraction of the pink pattern, the CPG converges directly, and relatively quickly, to the stable pink pattern.

If we follow the evolution of orbit 1 for a longer time, we can see how, finally, the orbit leaves the region close to the stable manifold of the saddle pattern. As it is shown in Fig. 6, after a very long transient time where the orbit stays close to the saddle pattern, the orbit convergences to stable green pattern. We observe how some neurons are adjusting slowly the bursting period (the black arrows on the voltage lines).

Right part of the Fig. 4 shows that for $v_{KS}^{th} = -25$ the only pattern present in the panel is the tripod gait. This generates that, in the subspace selected for the initial conditions, the orbits evolve quite rapidly towards the tripod pattern, which can be seen by the shape of the somewhat abrupt lines that form this right panel.

Despite all the information provided by this analysis, what we cannot know only with this technique is if there is any other stable pattern outside the studied manifold. To address this problem, we can use the *quasi-Monte Carlo sweeping* method explained at the beginning of the section, since this method searches for all stable patterns (with a sufficiently large basin of attraction) within the region with biological significance in the phase space. In Fig. 7 we show the results obtained combining this method with the spike-counting technique. On the horizontal plane we plot on black and white the biparametric plane (setting $v_K^{th} = 2$) using the spike-counting technique. Lighter gray colors correspond to a greater number of spikes in the periodic orbit. Over this biparametric plot we perform a complete analysis in two lines applying the quasi-Monte Carlo sweeping method. One vertical line with $v_{KS}^{th} = -26.5$ and one horizontal line with $I_{ext} = 35.5$. In the vertical planes each color corresponds with a different class of equivalence of detected patterns. We can observe that although the region can be longer or shorter, the sequence of colors (thus, behavior) is the same in both slices. We select the four main different routes to reach the tripod movement. Figs. 8 and 9 show some representative patterns inside the different routes, as well as the percentage of initial conditions that converge to that pattern within the analyzed set. The numbers of the hexagrams correspond to those in Fig. 7.

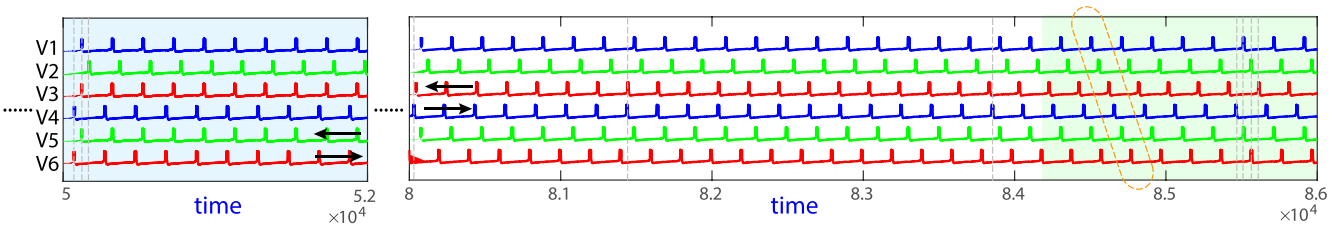

Fig. 6. Long time evolution of voltages of orbit 1 of the phase delay diagram of Fig. 5. The orbit remains very long time ($> 5 \cdot 10^4$ ms) close to the light blue saddle pattern following the stable manifold of the point and then converges to the stable green pattern dot.

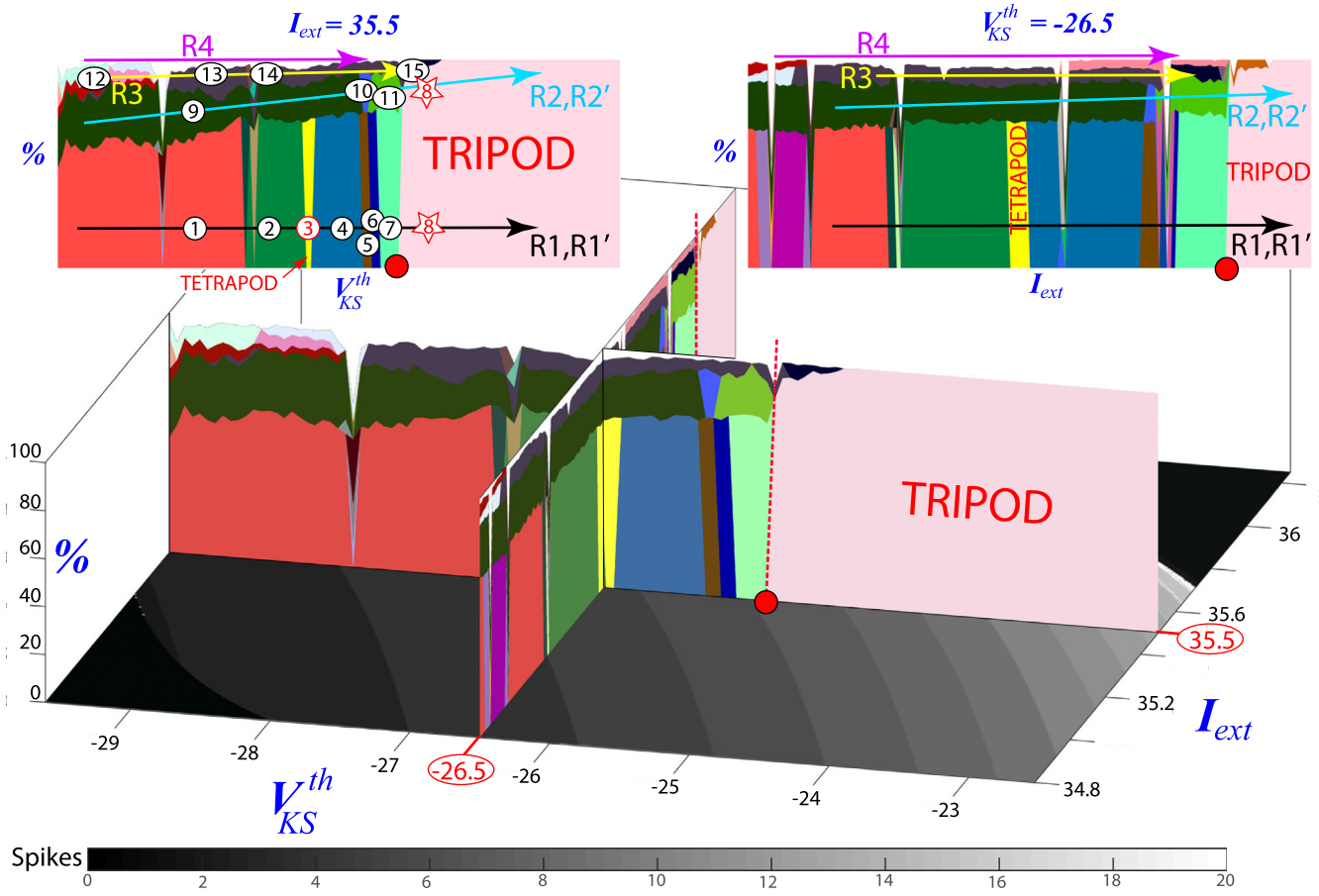

Fig. 7. On black and white the biparametric plane $v_K^{th} = 2$ using the spike-counting technique, and in color the two maps with the percentage of the different gaits corresponding to a vertical and a horizontal line on the parametric plane (v_{KS}^{th}, I_{ext}) applying the *quasi-Monte Carlo sweeping* method using 200 initial conditions for each parametric set. See text for explanation.

The most common gait is R1 and its symmetric one (R1′), since more than 60% of the initial conditions reach these configurations. The R1 route (see Fig. 8) starts from $d_{12} = 0.2 = d_{45}, d_{32} = 0.8 = d_{65}$ and a delay between central neuron of $d_{25} = 0.2$. In gait number –1– legs (N2) and (N4) are in swing at the same time, then (N3) and (N5) also go together and (N1) and (N6) do not swing at the same time. In gait –2– legs N1 and N6 do not swing at the same time but they match swinging for a while. In gait –3– N1 and N6 synchronize, the route reaches tetrapod gait. Therefore there are always four legs on the ground. The subsequent hexagrams are similar, but they are different gaits due to different overlapping of the bursting time interval of the neurons. For this reason we have plot some red dashed lines to remark if one leg swing after another or there are several legs swinging (see gaits –5– and –6–). While in gait –4– legs N1 and N6 swing during a while together, in –5– the match time is minimum and in –6– leg N1 do not swing at any time with N6 but a little bit with N3 and N5. This matching time is getting bigger until tripod gait, where they all three swing at the same time. R1′ route shows the symmetric hexagrams exchanging front to rear and right to left. The symmetric hexagram corresponds to the same class of equivalence, and so the percentages include both cases together. Note that, within this route, the tetrapod pattern appears as a circumstantial synchronization in the parametric evolution towards the tripod.

The R2 route (see Fig. 8) starts from a delay in every leg of 0.2. The sequence is completely different from route R1. We do not go through tetrapod because in every class there are always a moment where three legs are swinging. The route to tripod is different and shorter (in the sense of going through fewer states) because since there are already three legs synchronized, it only remains to synchronize one leg with a pair of synchronized legs. This route accumulates around 20% of the initial conditions.

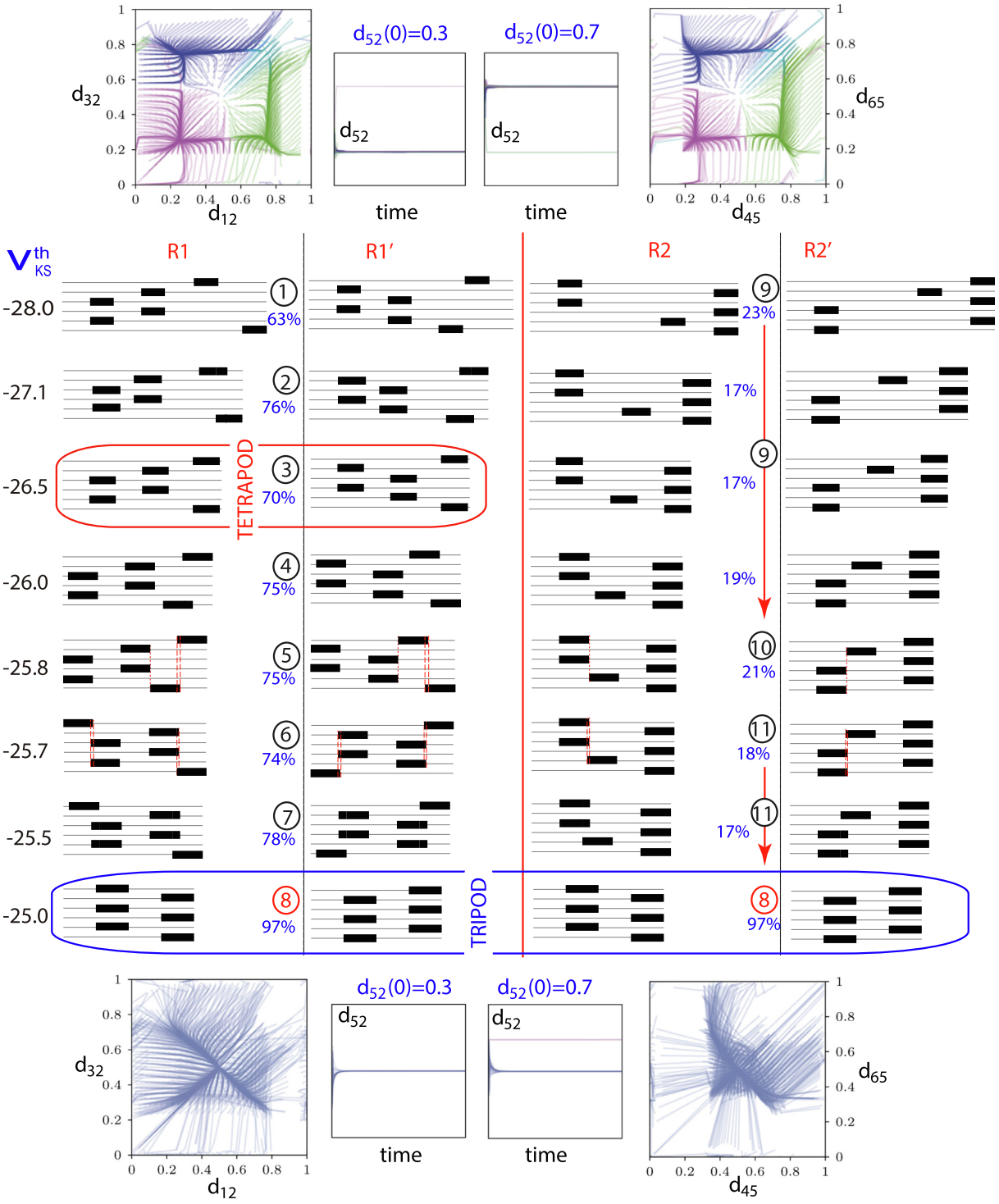

Fig. 8. On the top and on the bottom, two pictures with the lateral phase lag diagrams (left and right legs delays) corresponding to $v_{KS}^{th} = -28$ (top) and $v_{KS}^{th} = -25$ (bottom), both with $I_{ext} = 35.5$ and $v_K^{th} = 2$, and two central pictures with the temporal evolution of the phase lag between both central neurons for two sets of central initial delays. In the middle of the figure we show the different hexagrams for each class of equivalence on the routes R1 and R2 shown in Fig. 7, and their symmetric ones, towards the tripod gait.

The two remaining routes shown in Fig. 9 present two important differences with respect to the previous ones. On the one hand, the percentage of initial conditions that converge to any of them is much lower than the previous ones. On the other hand, the movement of the legs on the left side does not follow the same pattern as that of the legs on the right side. These routes correspond to patterns that have not been detected by the lateral phase lag analysis. In the other two routes (R1 and R2) both sides have the same behavior, but with different delays that give the different configurations. Note that although the model is symmetrical, it generates asymmetric stable patterns.

On the left of the Fig. 9 we show route R3 (as marked in Fig. 7). This route is made up of minor modifications in the synchronization of paired neurons. The two individually activated neurons do

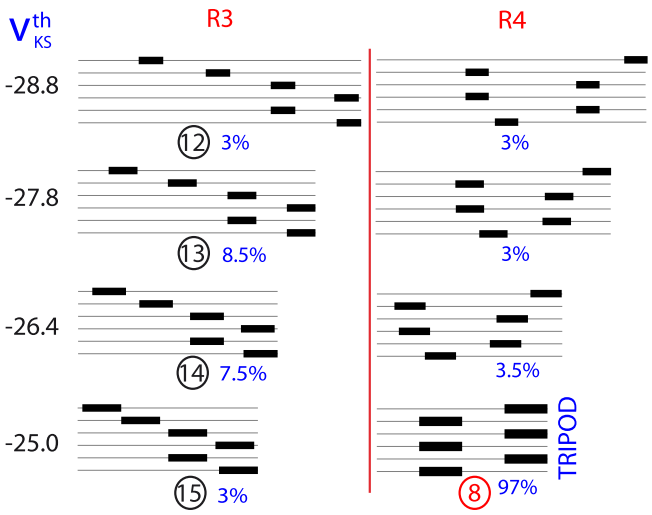

Fig. 9. On the left we show route R3 (as marked in Fig. 7) going also to $v_{KS}^{th} = -25$ on the line $I_{ext} = 35.5$. On the right of the figure we see route R4.

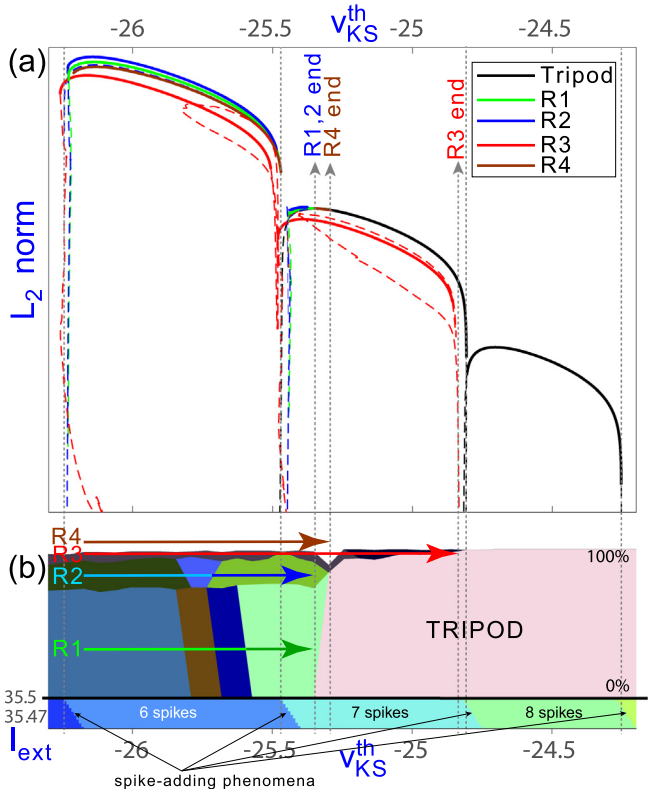

Fig. 10. (a) Bifurcation curves of the orbits (patterns) that configure the different routes. Each color represents a different route; solid lines mark stable periodic orbits, while dashed lines indicate unstable periodic orbits. (b) Top: map with the percentage of the different gaits corresponding to the line $I_{ext} = 35.5$ and $v_K^{th} = 2$ applying the quasi-Monte Carlo sweeping method. Bottom: Spike counting technique, for an isolated neuron, in a narrow strip parallel to the line of study.

not overlap with each other. Neither do the two blocks of pairs of neurons with each other. It is the only route of these four that does not end up collapsing with the tripod gait.

On the right of Fig. 9 we see route R4. The difference between this route and the R1′ is that N6 is between the two blocks of pairs of synchronized neurons. This makes the pattern not symmetrical and makes it impossible for the tetrapod to appear. However, as we will see in the next subsection, its limit case is the tripod, since both N1 and N6 move to the left until each one synchronizes with the corresponding block and forms the tripod pattern.

For $v_{KS}^{th} = -25$, 97% of the initial conditions reach the tripod gait and the remaining 3% reach state –15– showed in R3. This route R3 disappears soon after $v_{KS}^{th} = -25$ and then the only pattern observed is that of the tripod.

3.2. Origin and end of the different routes: bifurcation analysis

In the previous subsection we have seen how, by changing the v_{KS}^{th} or the I_{ext} parameters, the system goes from a situation in which four stable patterns coexist and, at least, one saddle pattern and another repulsive one (tripod), to another situation in which we only observe a single (now stable) pattern, the tripod. The observations made seem to indicate that the R1, R2 and R4 routes, as well as the saddle, converge towards the repulsor, making it stable. But is that really what happens? And what about R3?

In this subsection, through the analysis of the bifurcations that take place in the process of change, we will give an explanation from the point of view of the dynamical systems theory of the origin or disappearance of these patterns. To do this, we will use the AUTO software [23,24], which allows us to continue both stable and unstable orbits, as well as the bifurcations they experience. In this study we will focus on the line $I_{ext} = 35.5$. But, as we have previously observed, the process is analogous on other lines.

Fig. 10 has two panels. Panel (a) shows the different bifurcation curves of the orbits that configure the patterns of each route along the selected line (the vertical axis denotes the L_2 norm of AUTO). The colors of the curves differentiate each of the routes. Continuous and discontinuous curves represent stable and unstable orbits, respectively. Panel (b) shows at the top the percentages of initial

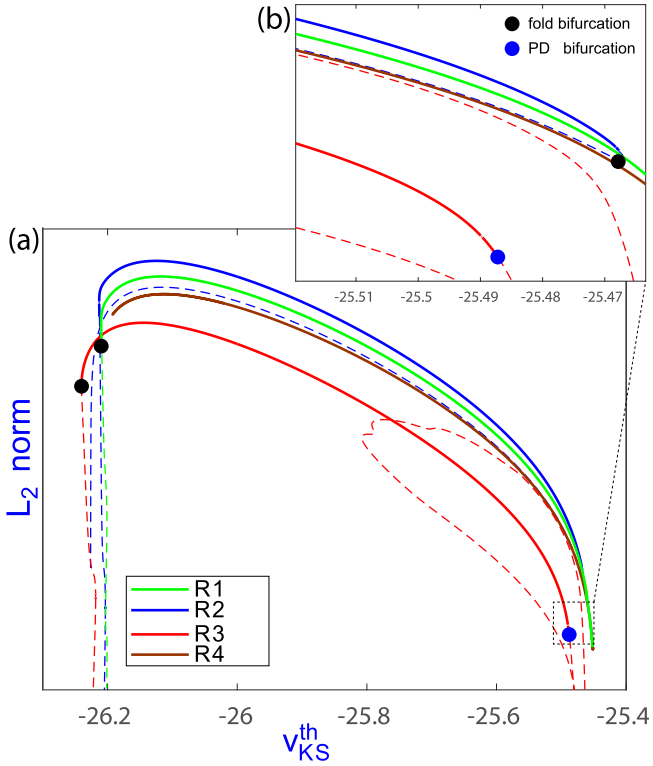

Fig. 11. (a) Magnification of the first lobe shown in Fig. 10. Inside this segment each neuron runs 6 spikes along its orbit. (b) Magnification of right bottom square marked in (a). Fold and period-doubling bifurcations are marked for some bifurcation curves.

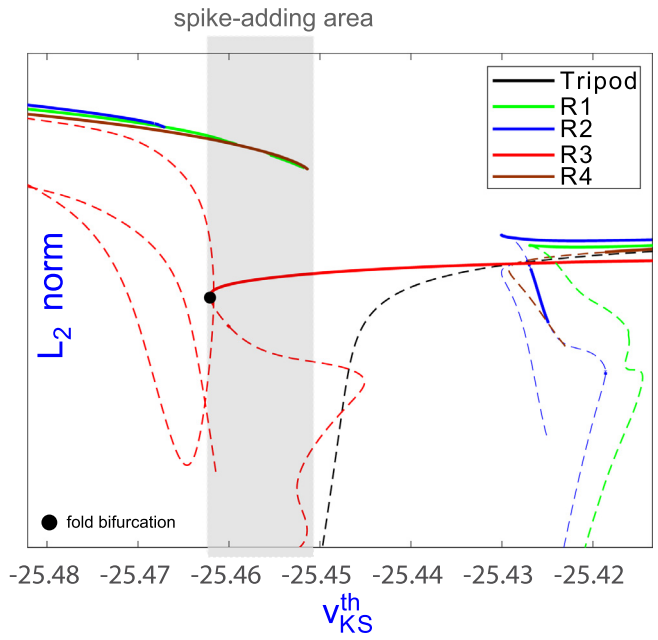

Fig. 12. Magnification of the spike-adding area between first and second lobes of Fig. 10 (corresponding to 6 and 7 spikes individual orbits, respectively). The region of coexistence between stable patterns with different number of spikes in their individual orbits is highlighted in gray.

conditions that converge to each route (with their different patterns) obtained with the quasi-Monte Carlo sweeping method. The spike-counting for an isolated neuron on a narrow biparametric strip appears at the bottom, the upper limit of which is the segment studied with the other two techniques. The superposition of the three pictures allows us to compare results obtained with different techniques, complementing each other and giving more complete and global information. Thus, we can see how the ends of the different routes determined by the quasi-Monte Carlo sweeping method correspond to the values where the corresponding bifurcation curves lose their stability (see Fig. 13 for more details). Moreover, despite the abrupt change in the number of spikes, and thus the orbit at the individual level of each neuron, most of the patterns existing in the network before the crisis generated by the discontinuous spike-adding phenomenon [30] reappear in the following lobe (see more details in the following figures). Finally, only the curve corresponding to the tripod gait appears in the last shown lobe. This curve is determined by the region where the isolated neuron orbits have 8 spikes. Next, we will detail what has been happening in the two previous lobes to arrive at this final situation.

Fig. 11 presents the evolution in the lobe generated by orbits with 6 spikes. This lobe shows the standard evolution (in the left lobes, outside of Fig. 10, the situation is similar). The patterns of each route are started from a fold bifurcation of limit cycles (different on each route), from which an unstable and a stable orbit arises. The latter is the one that configures the corresponding part of the route as the parameters change (in this line, v_{KS}^{th}). We can see how the first route that appears is R3, which is also the first to lose its stability, in this case in a period-doubling bifurcation. Routes R1 and R2 appear practically at the same time, however the fold bifurcation where R1 loses its stability is slightly more to the right than that of R2. Finally, route R4 appears, which is also the last one to become unstable, in a fold bifurcation a little more to the right than that of R1. Inside the lobe, the evolution of the stable part, which determines each pattern, is quite smooth.

As we have previously commented, the transition between one lobe with n spikes and the next, with $n+1$ spikes, is generated by a discontinuous spike-adding phenomenon [30]. This discontinuity is shown in Fig. 12, in which the orbits corresponding to 6 spikes disappear, and new ones appear with 7 spikes. As the appearance and disappearance is not simultaneous for the different routes, we can see how there is an area (highlighted in gray) in which R1 and R4 patterns, whose orbits have 6 spikes, coexist with R3 patterns formed by orbits with 7 spikes. In that region, for example, route R2 does not appear. Similarly, R3 does not appear to the left of that area and R1, R2 and R4 do not appear to the right. However, the interval where all this occurs is relatively small. We see here how it also appears, for the first time, a black dashed line corresponding to unstable tripod orbits. In the previous lobes it also exists, but in them it is always unstable (remember the repulsor detected with the lateral phase lag analysis). If we now look at Fig. 13, we can see in (b) a bifurcation point (magnified in (c)) where the tripod gait becomes stable. That point is a singular pitchfork bifurcation where R1 (green), R2 (dark blue) and saddle pattern (cyan) in Fig. 4 along with their symmetrical ones, all unstable, coalesce with the stable tripod pattern and only the unstable tripod pattern comes out. Note that the symmetrical patterns cannot be distinguished in these figures since their L_2 norm is the same. Here, the unstable branches of the R1 and R2 routes bifurcate from the tripod gait curve. Something similar occurs with the R4 route in another pitchfork bifurcation point a little lower in (b). In this case, only the R4 route (with its symmetrical one) collides with the tripod gait, which is already unstable, but whose unstable manifold increases its dimension at the bifurcation.

Although these three routes bifurcate from the tripod pattern, we consider they fully vanished when their pattern becomes unstable (a bit further than the pitchfork bifurcation where the tripod gait becomes stable). Due to this fact, there is a small area where the stable pattern of the tripod gait coexists with the stable patterns of the three routes (actually also with the R3 route). This fact had already been detected by the quasi-Monte Carlo sweeping method although the region is so small that it can be difficult to observe (see Fig. 7).

If we now focus our attention on route R3, we can see how this route continues along the lobe and becomes unstable at a period-doubling bifurcation in the spike-adding area, just as it happened in the previous lobe. The difference is that we have no longer been able to locate any stable orbit of this route beyond that value. Obviously, this does not mean that it does not exist; it may be that its basin of attraction is very small. But we hypothesize that once the tripod's basin of attraction has spread throughout the region of interest, which occurs when the only remaining alternative route (R3) becomes unstable, tripod no longer allows R3 to reappear in the next lobe. Note that, unlike what happens with the tetrapod gait, the tripod gait is not a circumstantial pattern, but it is a highly stable family of periodic orbits that evolves (just changing period and duty cycle) when system parameters change.

3.3. Asymmetric configurations

All the previous analyses have been done considering a highly symmetric CPG, both in the geometry and in the six neurons involved. As a preliminary study of the effects of using asymmetric configurations, we study some asymmetries on the geometry of the CPG, that is, we change the parameters c_i of the connections among the different neurons, but taking all the neurons the same. Obviously in Nature there are higher levels of asymmetry but a detailed analysis has to be done for each different configuration and this is far from the scope of this article. In Fig. 14 we illustrate the different configurations we simulate in this section, the symmetric one (front-rear and left–right symmetries), NET1 (left–right symmetry), NET2 (front-rear symmetry) and NET3 (totally asymmetric). For each asymmetric configuration we have perturbed randomly

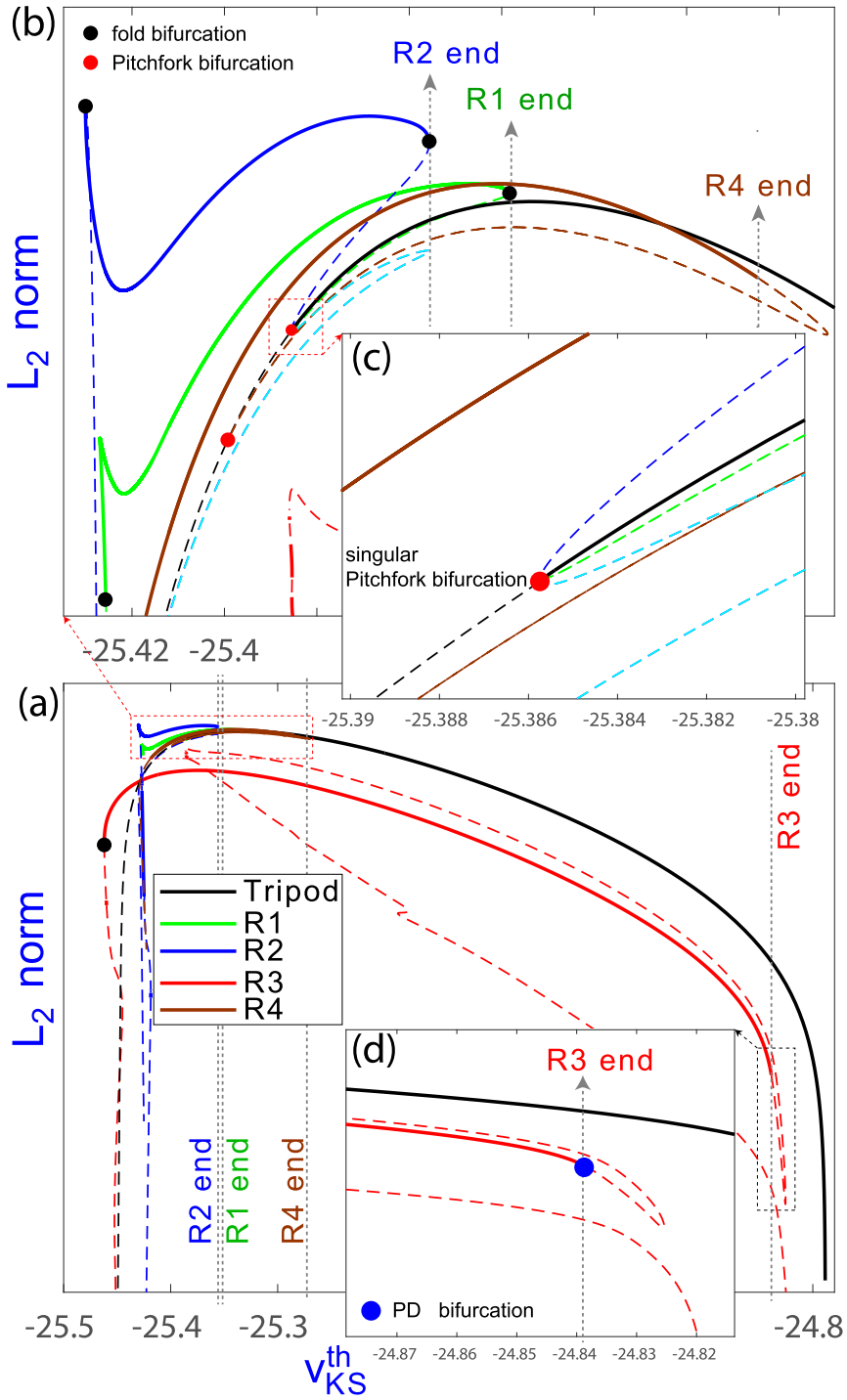

Fig. 13. Different magnifications of second lobe showing the ends of the four main pattern routes. (a) Complete lobe; (b) Left region with the ends of routes R1, R2 and R4; (c) Small region where routes R1, R2 and tripod gait collide; (d) Right region with the end of route R3. See explanation in the text.

the symmetric c_i parameters ($c_4 = c_7 = \frac{1}{2}, c_1 = c_2 = c_3 = c_5 = c_6 = 1$) by different maximum percentages. On the figure the coefficients c_i denote the original coefficients and $\tilde{c}_i$ and $\tilde{c}_i'$ the randomly perturbed ones.

In order to analyze the "robustness" of the four main routes studied in previous sections for the symmetric case (R1, R2, R3 and R4) we consider several cases of the asymmetric networks described in Fig. 14. In Fig. 15 we show some patterns of the asymmetric random network parameter configurations using as initial data the patterns of the symmetric case for the same parametric values. We have studied the parameter values $v_{KS}^{th} = -26, -25.5, -25$ and -23 with the fixed values $I_{ext} = 35.5$ and $v_K^{th} = 2$, that is, the area where the change to the dominant tripod gait occurs in the horizontal line of Fig. 7. The c_i coefficients have been perturbed a $1\%, 10\%$ and 100%, that is from small perturbations to a highly perturbed situation. The main conclusion of this figure is that the different routes are highly stable, being present for almost all cases. Only when the asymmetry and the allowed random perturbations are increased the observed patterns are different, although in some cases they are small modifications

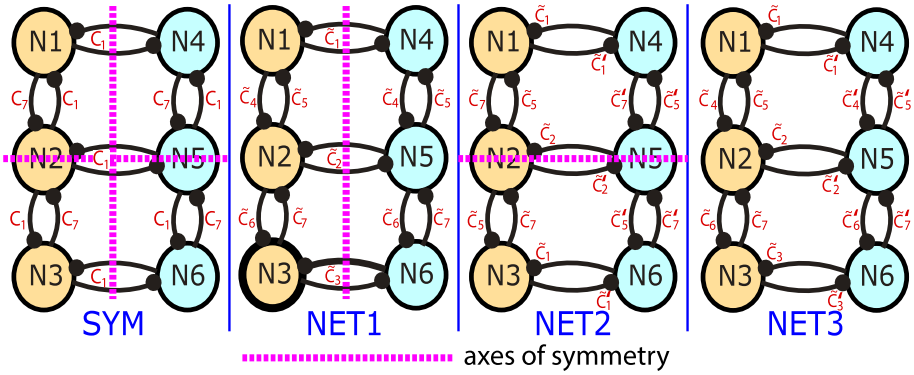

Fig. 14. Symmetric and asymmetric CPGs: symmetric (front-rear and left–right symmetries), NET1 (left–right symmetry), NET2 (front-rear symmetry) and NET3 (totally asymmetric). c_i denotes the original coefficients and $\tilde{c}_i$ and $\tilde{c}'_i$ the randomly perturbed coefficients.

of the standard patterns or the convergence simply goes to another route (or even patterns that were unstable in the symmetric case). In the Fig. 15 the cases that follow the same route have the same background color, whereas when a change is observed the background color is white.

Another remarkable fact is that in *all* cases, when the parameter v_{KS}^{th} grows, the patterns *always* go to the tripod gait, independently of the random perturbation we have added to the geometry of the network, and therefore this illustrates the metastability [25] and the reason of the ubiquity of the tripod pattern. Obviously more detailed analyses have to be done and it is part of our future research.

Once we have seen the four main routes are present in most of the CPG configurations we have considered, we study now the complete evolution along a parametric line (not just at several parametric values) in Fig. 16. In this case we study the horizontal parametric line $I_{ext} = 35.5$ applying the *quasi-Monte Carlo sweeping* method as in Fig. 7. At the top of Fig. 16 we show the symmetric case, and on the bottom an asymmetric one (NET3 of Fig. 14) with c_i coefficients perturbed randomly up to 50%. That is, we consider a highly perturbed configuration on the geometry of the CPG network. Fig. 15 seems to imply that small perturbations produce a behavior very similar to that of the symmetric case. So, we just focus on the highly perturbed case. The color figures show the percentage of the different gaits for the different parametric values. As Fig. 16 shows, the global behavior is similar but, obviously, not the same. In the asymmetrical sweep (bottom part of Fig. 16) we find striped colors. Those with northeast white stripes represent patterns similar to the corresponding ones in the symmetrical sweep but with small perturbations. Those with multicolor northwest stripes, represent patterns which can be seen as perturbations of the symmetrical ones encoded with the same colors; for example, region in $v_{KS}^{th} = -24$ has green and pink stripes which means that those patterns can be as in green region (see plot 7 in Fig. 8) or as in pink region but, in both cases, with a small perturbation (see $\sim$ TRIPOD pattern in the asymmetric net). Finally, those with darker horizontal lines are patterns perturbed from the symmetrical case but with a front-rear legs symmetry applied in one of the sides of the network. These patterns did not appear in the symmetrical case. Of course, solid colors are the same patterns in both plates, except for the light gray areas on bottom plate, representing (irregular) patterns distinct enough from any of the symmetric case to be in its own class. We have chosen to highlight the added noise to the patterns but some of the striped areas are very similar to the regular ones. The two main patterns are illustrated at the values $v_{KS}^{th} = -28, -27, -26, -25, -24$ and -23 showing the coincidence at most cases but close to the value of the appearance of the tripod gait as more similar (but not exactly the same) configurations are present.

What is remarkable is firstly the applicability of the *quasi-Monte Carlo sweeping* method to describe the evolution. Secondly how quite symmetric patterns are able to come in the asymmetric case. And, finally, the similarity of the two cases (with obvious differences) in the sense that the main routes are present, the main changes are at similar parametric values and the appearance of the tripod (or quasi-tripod) gait occurs at close parametric values. Therefore, an important remark is that a detailed study of the symmetric case provides the key analysis to understand the asymmetric ones.

3.4. Location of tripod limit curve

The previous section has shown that the symmetric case provides basic information to take into account when we study generic configurations, and also it has been shown that the tripod gait is present in all the CPG cases studied. Therefore, it is relevant to focus our attention in locating where this ubiquitous tripod gait [25] begins to appear in the parameter space.

Fig. 7 shows two points (marked with red dots), in the (v_{KS}^{th}, I_{ext})-plane for $v_K^{th} = 2$, where the tripod gait suddenly appears. Moreover, once the tripod gait is present, it quickly becomes the dominant gait and the rest of them have become it (routes R1, R2 and R4) or simply disappear (route R3). Thus, there should be a boundary line on this plane where on one side there are no tripod gaits and in the other side it is the dominant one. This line of bifurcation, the *Tripod gait limit curve* (see Fig. 17), can be computed with a variation of the algorithm used to compute Fig. 7. The algorithm runs as follows: Firstly, set `is_tripod`(v_{KS}^{th}) = 1 if any of 20 initial conditions (selected through the *quasi-Monte Carlo sweeping* method above described) is a tripod gait pattern, and to 0 otherwise. In this process, all integrations run in parallel with an adaptive transient time: for each initial condition we repeat the following up to 20 times. Integrate for 10 s (transient time) and check if the orbit reproduces a pattern in the next 5 s. If it is not, repeat the process. If after 300 s there is no pattern orbit, it is not a tripod. If a pattern is found, we check if it is a tripod.

Now, we have to start with an initial guess of the point of the tripod gait limit for the lowest value of parameters we consider (in our case $I_{ext} = 34.5$). With the *quasi-Monte Carlo sweeping* method we detect the value $I_{ext} = 34.5$ and $v_{KS}^{th} = -22$, and with this initial point of the curve we repeat the next steps until we reach a predefined maximal value $I_{ext} = 36.4$:

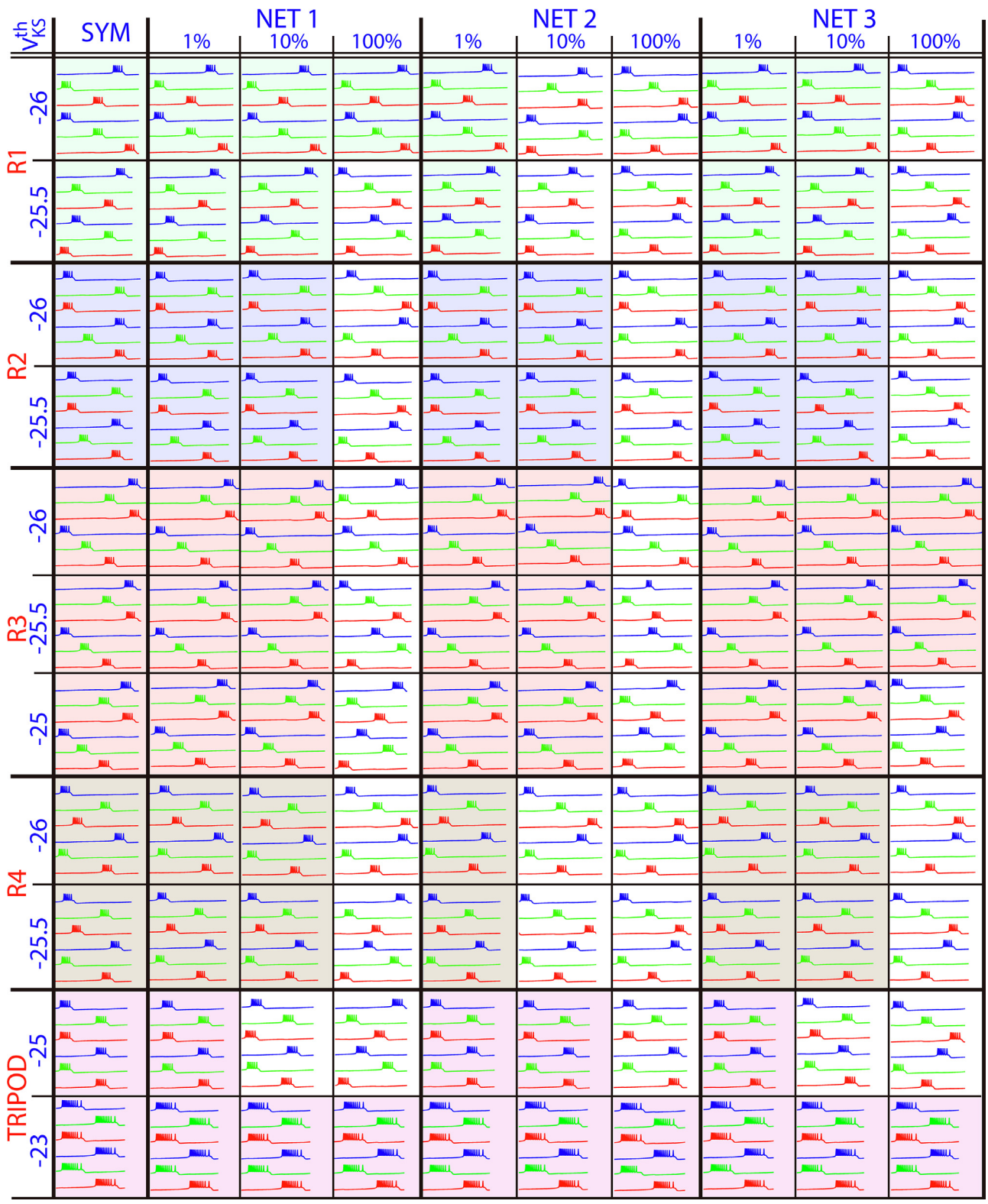

Fig. 15. Some patterns of the asymmetric random network parameter configurations of Fig. 14 using as initial data the patterns of the symmetric case. Colored background represents that the pattern of the perturbed network matches that of the original symmetric network.

1. *Initial interval:* We need to compute an interval $[a, b]$ such that `is_tripod(a)` $= 0$ and `is_tripod(b)` $= 1$. To do so, it is enough to set a or b to the current v^{th}_{KS} depending on `is_tripod(`v^{th}_{KS}`)` = 1 and to move the other extreme in steps of 0.1 to the left or right to reach a point fulfilling the needed condition.

2. *Bisection-like procedure:* We perform a bisection algorithm on `is_tripod` with a precision of 0.001.

3. *Update:* Increase I_{ext} by 0.01 (unless we reach the maximal selected value $I_{ext} = 36.4$, where we stop the algorithm), and go back to Step 1. The initial guess for v^{th}_{KS} in the next step will be the current one.

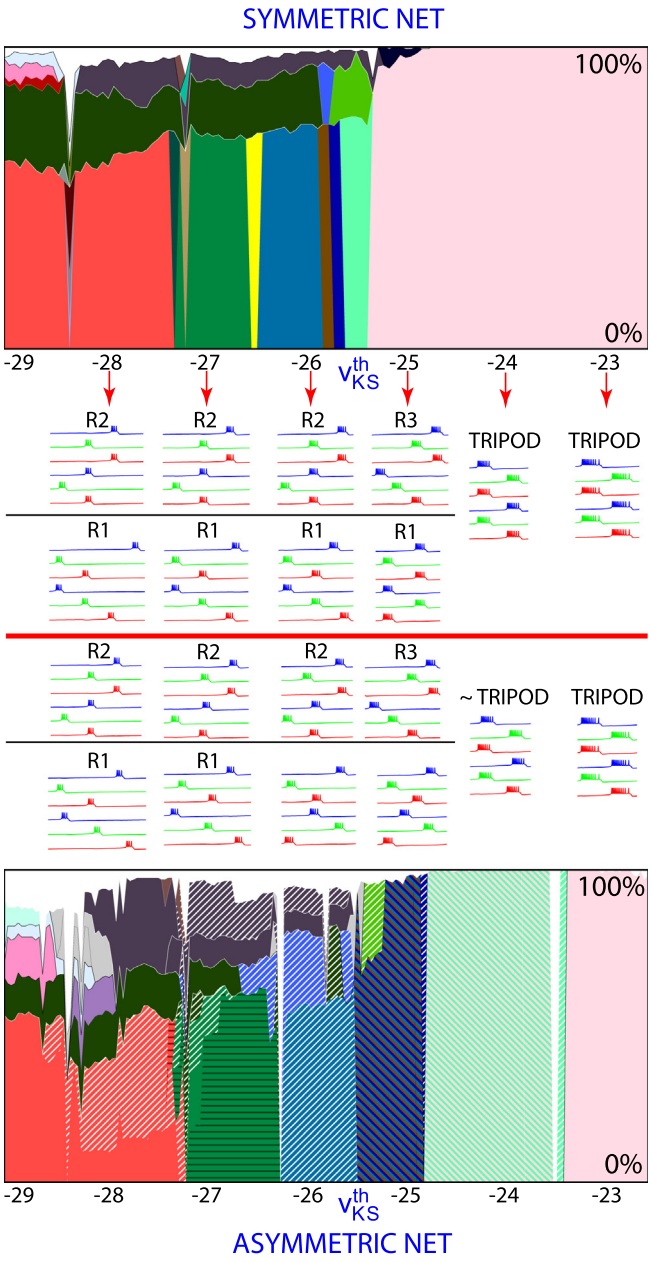

Fig. 16. The two maps, considering the symmetric and a totally asymmetric CPG (NET3 of Fig. 14) with c_i coefficients perturbed randomly up to 50%, with the percentage of the different gaits corresponding to the horizontal line $I_{ext} = 35.5$ applying the *quasi-Monte Carlo sweeping* method. The two main patterns are illustrated at the values $v^{th}_{KS} = -28, -27, -26, -25, -24$ and -23. See text for explanation.

This methodology produced the black curve drawn in Fig. 17 superimposed on the single neuron spike-counting diagram. There, we can see how this bifurcation tends to stick to the spike adding bifurcation of the single neuron, making it wavy on the region were more bifurcations cluster.

At a first glance, the two elections made in the algorithm, the number of initial conditions and the criteria to decide when `is_tripod` is 0 or 1, would produce different curves. But it is not the case, we have tried with 200 initial conditions and with other two different criteria: all simulations should be tripod to make $\texttt{is\_tripod}(v^{th}_{KS}) = 1$, and half the sample should be tripod for the same result. In all cases, the curve is essentially the same (asking for more tripods slightly move it to the right, cf. Figs. 7 and 13). Fig. 17 also displays the bifurcation (red dots) and the lines $I_{ext} = 35.5$ and $v^{th}_{KS} = -26.5$ (dashed white) of Fig. 7.

We can extend this computation to parameter space depicted in the middle picture of Fig. 3, just running the above algorithm for distinct values of v^{th}_{K}. Fig. 18 shows the actual computed surface in this parameter space. This suggests that there is a huge part of global parameter space where the tripod pattern is ubiquitous, only changing its duty cycle length and frequency. This region contains the parameters producing high number of spikes, while lower number of spikes might produce a richer variety of patterns.

4. Conclusions

In this paper we have combined different numerical techniques recently developed for small networks to analyze the movement patterns of insects. We have considered a CPG model of insect movement that consists of six coupled neurons developed by Ghigliazza and Holmes (2004) for motoneurons of cockroaches, and we have initially assumed a symmetrical leg configuration. Previous studies in literature analyzed reduced models of dimension two obtained using phase resetting curves and averaging theory, but in this paper we have analyzed the complete model with the help of the numerical techniques. Firstly, we have shown how the preliminary study of the model of an isolated neuron provides us with valuable information to determine the three parametric region of interest in the subsequent analysis of the CPG. The results obtained by this new methodology have shown different routes in a biparametric phase space to finally achieve a highly stable tripod gait movement. Due to the model configuration, most of the observed patterns follow a route made by symmetric gaits that lead to the tripod gait. In addition, we have also detected other (minor) routes that present non-symmetrical gaits, giving the interesting fact that these gaits are also possible in symmetric model settings. In this article the bifurcations of the main pattern routes detected in the parameter space have been studied in detail using continuation techniques via the AUTO software. This study has revealed the mechanisms that explain how the observed patterns appear or disappear, and what is more relevant, why for large values of some parameters only the tripod gait is present. Besides, using the symmetric CPG case as the basic information, we have studied several asymmetric configurations of the CPG in order to see the robustness of the different pattern routes, being most of them highly robust as they are always present. Taking into account that most of the routes lead to tripod gait, and the rest simply disappears, due to some bifurcations, we have introduced an algorithm to locate the limit of the tripod gait in a three dimensional parameter space. With this technique we have discovered that there is a large region in the parameter space where the tripod pattern is ubiquitous and highly dominant, only changing its duty cycle length and frequency, and therefore, this mathematical analysis of the insect CPG also explains why the tripod gait is the gait of movement to run fast in generic insect movement.

CRediT authorship contribution statement

R. Barrio: Investigation, Methodology, Software, Validation, Writing - original draft, Writing - review & editing. **Á. Lozano:** Investigation, Methodology, Software, Validation, Writing - review & editing. **M.A. Martínez:** Validation, Writing - original draft, Writing - review & editing. **M. Rodríguez:** Validation, Software, Writing

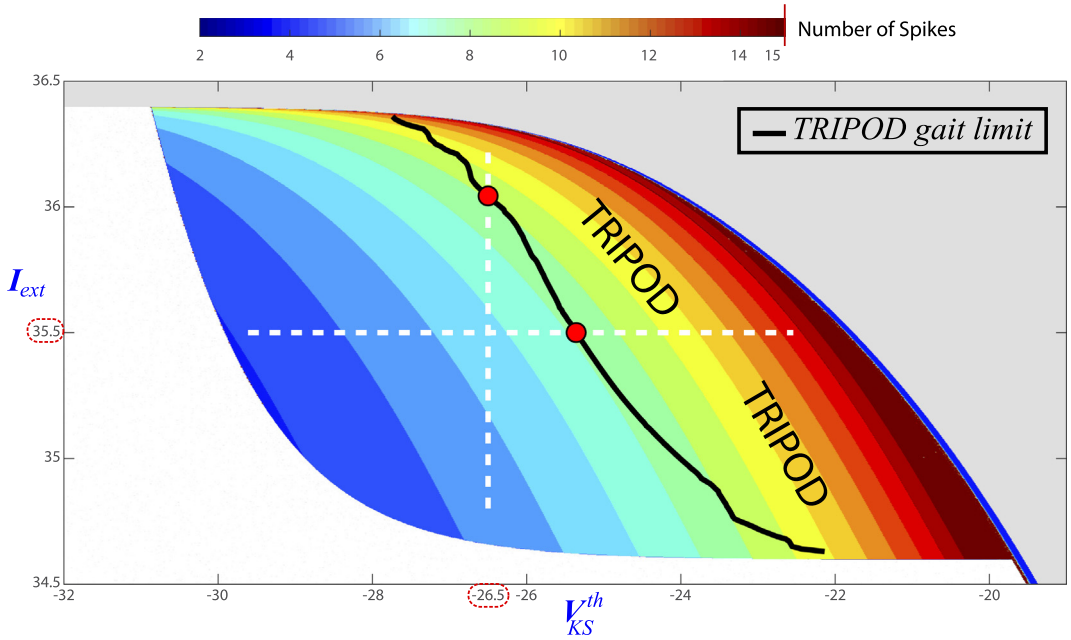

Fig. 17. Biparametric (v_{KS}^{th}, I_{ext}) plane (with $v_K^{th} = 2$) using the spike-counting technique and the computed line (black) that gives the dominant tripod gait limit. The white dashed lines correspond to the histograms of Fig. 7 ($I_{ext} = 35.5$ and $v_{KS}^{th} = -26.5$) and with the red dots that point the tripod limit on that lines.

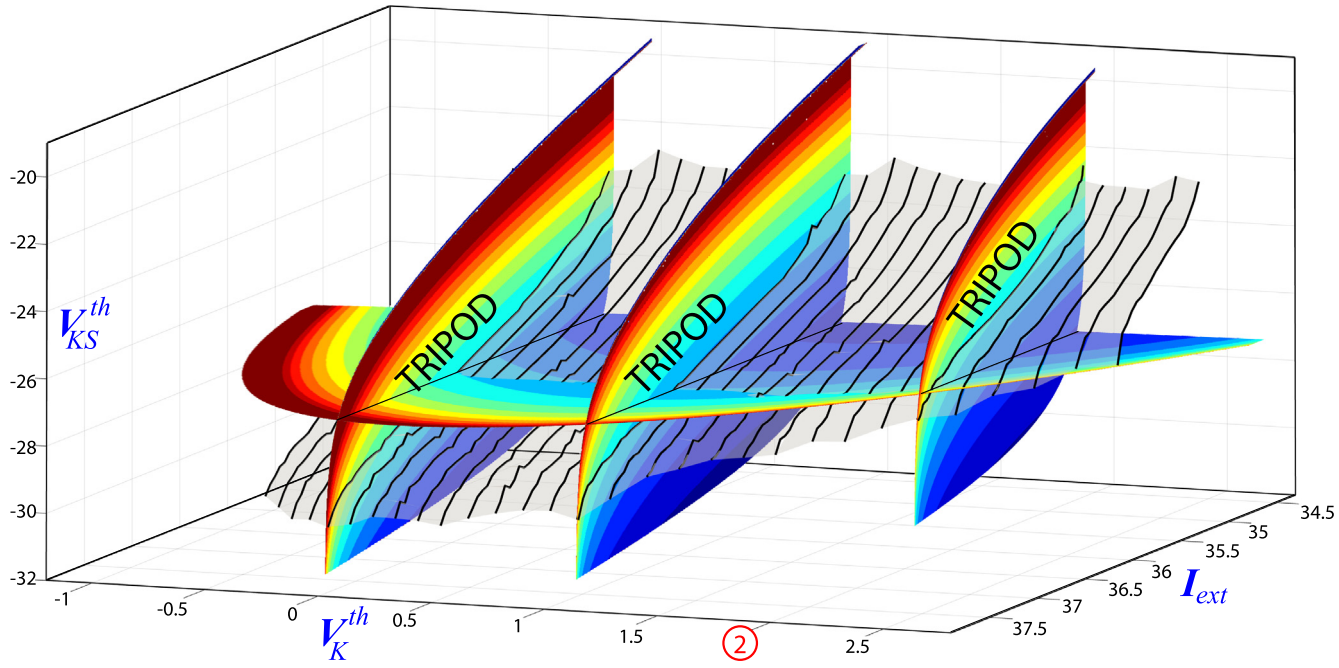

Fig. 18. The tripod gait limit surface in the $(v_K^{th}, v_{KS}^{th}, I_{ext})$ space with the spike-counting slices (Fig. 3). Slice $v_K^{th} = 2$ (in red) is the plane depicted in Fig. 17. Region above the surface is dominated by the tripod gait.

- review & editing. **S. Serrano:** Investigation, Methodology, Software, Validation, Writing - original draft, Writing - review & editing.

Declaration of Competing Interest

The authors declare that they have no known competing financial interests or personal relationships that could have appeared to influence the work reported in this paper.

Acknowledgments

The authors thank the reviewers for their comments that have helped to improve the article. RB and SS have been supported by the Spanish Ministry of Economy and Competitiveness (grant PGC2018-096026-B-I00). MAM has been supported by the Spanish Ministry of Economy and Competitiveness (grant DPI2016-75458-R). RB, MAM and SS have been supported by the European Social Fund (EU) and Aragón Government (grant LMP124-18 and group E24-17R). RB, ÁL, MAM and SS have been supported by the Univer-

sity of Zaragoza-CUD (grant UZCUD2019-CIE-04). ÁL has been supported by the Spanish Ministry of Economy and Competitiveness (grant MTM2016-77642-C2-2-P) and European Social Fund (EU) and Aragón Government (group E22-17R).

Appendix A

The neuron and CPG model used in this paper follows the model developed by Ghigliazza and Holmes [14,22]. The auxiliary ionic current functions used in (1) are defined by

$$\begin{aligned} I_{Ca}(v) &= g_{Ca}\, n_\infty(v)(v-E_{Ca}),\\ I_K(v,m) &= g_K\, m(v-E_K),\\ I_L(v) &= g_L(v-E_L),\\ I_{KS}(v,w) &= g_{KS}\, w(v-E_K). \end{aligned}$$

g_* is the maximal conductance and acts as a scaling factor, n, m and w are gating variables and E_* is the Nernst potential and fixes the unique value of the voltage for which the current vanishes.

The term I_{syn} is considered zero in case of an isolated neuron and, in the case of connected neurons, the different values of the extra current $(I_{syn})_i$ for each neuron potential v_i are:

$$\begin{aligned} (I_{syn})_1 &= c_1 g_{syn} s_4(v_1 - E_s^{post}) + c_5 g_{syn} s_2(v_1 - E_s^{post}),\\ (I_{syn})_2 &= c_2 g_{syn} s_5(v_2 - E_s^{post}) + c_4 g_{syn} s_1(v_2 - E_s^{post})\\ &\quad + c_7 g_{syn} s_3(v_2 - E_s^{post}),\\ (I_{syn})_3 &= c_3 g_{syn} s_6(v_3 - E_s^{post}) + c_6 g_{syn} s_2(v_3 - E_s^{post}),\\ (I_{syn})_4 &= c_1 g_{syn} s_1(v_4 - E_s^{post}) + c_5 g_{syn} s_5(v_4 - E_s^{post}),\\ (I_{syn})_5 &= c_2 g_{syn} s_2(v_5 - E_s^{post}) + c_4 g_{syn} s_4(v_5 - E_s^{post})\\ &\quad + c_7 g_{syn} s_6(v_5 - E_s^{post}),\\ (I_{syn})_6 &= c_3 g_{syn} s_3(v_6 - E_s^{post}) + c_6 g_{syn} s_5(v_6 - E_s^{post}). \end{aligned}$$

In this paper (as in [26]), we assume (except for the asymmetric configurations of SubSection 3.3) contralateral symmetry (between left and right side) and the balance conditions

$$c_1 + c_5 = c_2 + c_4 + c_7 = c_3 + c_6,$$

and

$$c_4 = c_7, \quad c_5 = c_6, \quad c_1 = c_3.$$

So, by symmetry, we do not differentiate forward and backward movements. Moreover, and as a particular example, we have set their values to

$$c_4 = c_7 = \frac{1}{2}, \qquad c_1 = c_2 = c_3 = c_5 = c_6 = 1.$$

The different time scales and steady state gating variables are

$$\begin{aligned} \tau_m(v) &= \operatorname{sech}\left(k_{0_K}(v - v_K^{th})/2\right),\\ \tau_w(v) &= \operatorname{sech}\left(k_{0_{KS}}(v - v_{KS}^{th})/2\right),\\ m_\infty(v) &= \left(1 + e^{-2k_{0_K}(v - v_K^{th})}\right)^{-1},\\ w_\infty(v) &= \left(1 + e^{-2k_{0_{KS}}(v - v_{KS}^{th})}\right)^{-1},\\ n_\infty(v) &= \left(1 + e^{-2k_{0_{Ca}}(v - v_{Ca}^{th})}\right)^{-1},\\ s_\infty(v) &= \frac{T_{max}}{1 + e^{-k_s(v - E_s^{pre})}}. \end{aligned}$$

v_*^{th} represents the threshold voltage and affects location and values of extrema. Finally the slope k_{0_*} determines the extend of the transition region from the inactive to the active state.

Most of the parameters values that we use along the paper are taken from [14]. Parameters in boldface have been used as study parameters and their values are given throughout the paper.

$$\begin{array}{ccc} C = 1.2, & E_{Ca} = 120.0, & E_K = -80.0,\\ E_L = -60.0, & \delta = 0.005, & \epsilon = 4.9,\\ g_{Ca} = 4.4, & g_K = 8.0, & g_{KS} = 0.15,\\ g_L = 2.0, & k_{0_{KS}} = 0.4, & k_{0_K} = 0.1,\\ E_s^{pre} = 2.0, & T_{max} = 0.002, & \alpha = 5000.0,\\ \beta = 0.18, & g_{syn} = 0.015, & k_s = 0.22,\\ E_s^{post} = -70.0, & \mathbf{k_{0_{Ca}}}, & \mathbf{v_{Ca}^{th}},\\ \mathbf{v_{KS}^{th}}, & \mathbf{I_{ext}}, & \mathbf{v_K^{th}}. \end{array} \tag{2}$$

References

[1] P. Ashwin, Symmetric chaos in systems of three and four forced oscillators, Nonlinearity 3 (3) (1990) 603–617.
[2] P. Ashwin, O. Burylko, Y. Maistrenko, Bifurcation to heteroclinic cycles and sensitivity in three and four coupled phase oscillators, Physica D 237 (4) (2008) 454–466.
[3] M. Aguiar, P. Ashwin, A. Dias, M. Field, Dynamics of coupled cell networks: Synchrony, heteroclinic cycles and inflation, Journal of Nonlinear Science 21 (2) (2011) 271–323.
[4] M.G. Rosenblum, A.S. Pikovsky, J. Kurths, Phase synchronization in driven and coupled chaotic oscillators, IEEE Transactions on Circuits and Systems I: Fundamental Theory and Applications 44 (10) (1997) 874–881.
[5] E. Marder, D. Bucher, Central pattern generators and the control of rhythmic movements, Current Biology 11 (23) (2001) R986–R996.
[6] A. Selverston, Model Neural Networks and Behavior, Springer, Berlin, 1985.
[7] T. Bal, F. Nagy, M. Moulins, The pyloric central pattern generator in crustacea: a set of conditional neural oscillators, Journal of Comparative Physiology A 163 (1996) 715–727.
[8] E. Marder, R. Calabrese, Principles of rhythmic motor pattern generation, Physiological Reviews 76 (1996) 687–717.
[9] E. Ott, T.M. Antonsen, Low dimensional behavior of large systems of globally coupled oscillators, Chaos 18 (3) (2008), 037113.
[10] R. Barrio, Á. Lozano, M. Rodríguez, S. Serrano, Numerical detection of patterns in CPGs: Gait patterns in insect movement, Communications in Nonlinear Science and Numerical Simulation 82 (2020), 105047.
[11] A. Ayali, A. Borgmann, A. Büschges, E. Couzin-Fuchs, S. Daun-Gruhn, P. Holmes, The comparative investigation of the stick insect and cockroach models in the study of insect locomotion, Current Opinion in Insect Science 12 (2015) 1–10.
[12] S. Fujiki, S. Aoi, T. Funato, N. Tomita, K. Senda, K. Tsuchiya, Hysteresis in the metachronal-tripod gait transition of insects: A modeling study, Physical Review E 88 (2013), 012717.
[13] R. Ritzmann, S.N. Zill, Neuroethology of Insect Walking, Scholarpedia 8 (9) (2013) 30879.
[14] R. Ghigliazza, P. Holmes, A minimal model of a central pattern generator and motoneurons for insect locomotion, SIAM Journal on Applied Dynamical Systems 3 (4) (2004) 671–700.
[15] R. Campos, V. Matos, C. Santos, Hexapod locomotion: A nonlinear dynamical systems approach, in, IECON 2010–36th Annual Conference on IEEE Industrial Electronics Society (2010) 1546–1551.
[16] F. Tedeschi, G. Carbone, Design issues for hexapod walking robots, Robotics 3 (2) (2014) 181–206.
[17] C. Ferrell, A comparison of three insect-inspired locomotion controllers, Robotics and Autonomous Systems 16 (2) (1995) 135–159.
[18] J.C. Spagna, D.I. Goldman, P.-C. Lin, D.E. Koditschek, R.J. Full, Distributed mechanical feedback in arthropods and robots simplifies control of rapid running on challenging terrain, Bioinspiration & Biomimetics 2 (1) (2007) 9–18.
[19] J.J. Collins, I. Stewart, Hexapodal gaits and coupled nonlinear oscillator models, Biological Cybernetics 68 (4) (1993) 287–298.
[20] F. Herrero-Carrón, F.B. Rodríguez, P. Varona, Bio-inspired design strategies for central pattern generator control in modular robotics, Bioinspiration & Biomimetics 6 (1) (2011), 016006.
[21] D.M. Wilson, Insect walking, Annual Review of Entomology 11 (1) (1966) 103–122.
[22] R. Ghigliazza, P. Holmes, Minimal models of bursting neurons: How multiple currents, conductances, and timescales affect bifuraction diagramgs, SIAM Journal on Applied Dynamical Systems 3 (4) (2004) 636–670.
[23] E. Doedel, AUTO: a program for the automatic bifurcation analysis of autonomous systems, Congruent Number 30 (1981) 265–284.
[24] E.J. Doedel, R. Paffenroth, A.R. Champneys, T.F. Fairgrieve, Y.A. Kuznetsov, B.E. Oldeman, B. Sandstede, X.J. Wang, Auto2000, http://cmvl.cs.concordia.ca/auto..
[25] E. Reches, D. Knebel, J. Rillich, A. Ayali, B. Barzel, The metastability of the double-tripod gait in locust locomotion, iScience 12 (2019) 53–65.
[26] Z. Aminzare, V. Srivastava, P. Holmes, Gait transitions in a phase oscillator model of an insect central pattern generator, SIAM Journal on Applied Dynamical Systems 17 (1) (2018) 626–671.
[27] M. Storace, E. de Linaro, Lange: The Hindmarsh-Rose neuron model: Bifurcation analysis and piecewise-linear approximations, Chaos 18 (2008), 033128.

[28] R. Barrio, A. Shilnikov, Parameter-sweeping techniques for temporal dynamics of neuronal systems: case study of Hindmarsh-Rose model, Journal of Mathematical Neuroscience 1 1 (6) (2011) 1–6, 22.
[29] J.H. Halton, On the efficiency of certain quasi-random sequences of points in evaluating multi-dimensional integrals, Numerische Mathematik 2 (1) (1960) 84–90.
[30] R. Barrio, S. Ibáñez, L. Pérez, S. Serrano, Spike-adding structure in fold/hom bursters, Communications in Nonlinear Science and Numerical Simulation 83 (2020), 105100.

ROBERTO BARRIO received the B.S. and Ph.D. degrees from the University of Zaragoza, Spain in 1992 and 1997, respectively, all in applied mathematics. He is currently a full Professor of department of Applied Mathematics, University of Zaragoza, Spain. His current research interests include optimization techniques, numerical analysis, mathematical neuroscience, biomathematics, dynamical systems and computational dynamics. He has authored or co-authored over 120 technical papers in different fields of applied mathematics in renowned international journals and conferences. He is currently an Editor of the journals Communications in Nonlinear Science and Numerical Simulation, Applied Mathematics and Computation, Frontiers in Applied Mathematics and Statistics, PlosONE.

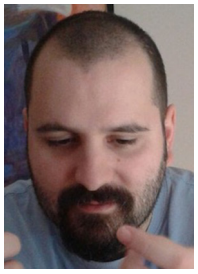

ÁLVARO LOZANO received his BSc + MSc and PhD in Mathematics from the University of the Basque Country in 2002 and 2008 respectively. He is currently Associate Professor at Centro Universitario de la Defensa AGM. His background is in topological dynamics and his current research interests are low-dimensional topology, networks, dynamical systems and its applications.

M. ANGELES MARTÍNEZ received the B.S degree in physics from the University of Zaragoza, Spain in 2002 and the Ph.D. degree from the University of Granada in 2008 within a doctoral program of physics and mathematics. She has been engaged in different projects both on Applied Physics and Applied Mathematics and since 2016 she is Lecturer at the department of Applied Mathematics in the Engineering School of the University of Zaragoza, Spain. Her current research interest are mainly dynamical systems, biomathematics and computational dynamics.

MARCOS RODRÍGUEZ got his PhD in Applied Mathematics in 2011. After that he got a position in the Centro Universitario de la Defensa de Zaragoza, where he continued his in computer science and neuroscience while teaching maths to undergraduate students of engineering. Nowadays he is a permanent teacher of in the public education system of Aragón, Spain, where he continues his research in both areas.

SERGIO SERRANO received the B.S. and Ph.D. degrees from the University of Zaragoza, Spain in 1998 and 2003, respectively, all in applied mathematics. He completed his doctorate in the CNES (National Center for Space Studies, Toulouse, France), a center with which he enjoyed a research fellowship for three years. He is currently Associate Professor of department of Applied Mathematics, University of Zaragoza, Spain. His main research interests are in biomathematics and mathematical neuroscience, numerical analysis, celestial mechanics and dynamical systems. His research has been expounded in around 50 publications and 70 presentations in congresses and it was funded by around 30 research projects.